



Full length article

# Blue phosphorene monolayers as potential nano sensors for volatile organic compounds under point defects

Suyang Sun<sup>a</sup>, Tanveer Hussain<sup>b,\*</sup>, Wei Zhang<sup>a</sup>, Amir Karton<sup>b</sup><sup>a</sup> Center for Advancing Materials Performance from the Nanoscale, State Key Laboratory for Mechanical Behavior of Materials, Xi'an Jiaotong University, Xi'an 710049, PR China<sup>b</sup> School of Molecular Sciences, University of Western Australia, Perth, WA 6009, Australia

## ARTICLE INFO

## Keywords:

DFT  
Gas sensing  
2D materials  
Substitution defects  
Vacancy defects

## ABSTRACT

Based on spin-polarized DFT calculations, we have studied the interaction mechanism of recently synthesized blue phosphorene (BlueP) monolayers towards selected key volatile organic compounds (VOCs) such as acetone, ethanol and propanal. Our binding energy analysis shows that pristine BlueP weakly binds the VOCs and that this binding does not appreciably change the electronic properties of the monolayer – a prerequisite for any sensing material. However, mono, di, and tri-vacancy defects and Si/S-substitutional doping significantly enhance the binding energies with VOCs. Density of state (DOS) calculations show that upon adsorption of VOCs, mono-vacancy and S-substituted BlueP monolayers undergo a major change in electronic structure, which make them potential candidates for VOCs sensing materials. By contrast, binding of VOCs to di- and tri-vacancy and Si-substitution sites does not alter the electronic structure of BlueP monolayers drastically, therefore, are not qualified for VOCs sensing applications.

## 1. Introduction

The detection of volatile organic compounds (VOCs) has become an important task, because high concentrations of VOCs in indoor air may be harmful to human health [1–5]. VOCs are organic compounds that have low boiling points and thus high vapor pressures at room temperature. A wide range of commonly used materials may release significant amounts of VOCs into indoor air [5], some of which are identified to be toxic and carcinogenic even at sub-ppb concentrations [1,6]. Therefore, it is important to design efficient sensors capable of detecting and capturing VOCs.

Semiconductor gas-sensors based on metal oxides are widely used to detect VOCs by monitoring the change in their electronic conductivity before and after the adsorption of gas molecules [6–11]. However, the conventional semiconductor sensors have limited resolution at the ppm level because of size and shape effects [10]. In addition, another fundamental reason limiting the resolution of such devices is the intrinsic noise due to the thermal motion of charges and defects, which may exceed the signal of the target molecules [12].

One approach for improving the resolution of semiconductor sensors is utilizing nanotechnologies. Metal oxide nanostructures offer a larger surface-to-volume ratio, i.e. more adsorption sites for the target gas molecules, and consequently higher sensitivity than conventional

materials. For example, Pt-decorated In<sub>2</sub>O<sub>3</sub> nanoparticles can reach up to ppb resolution [6,13]. Another way to improve the resolution of semiconductor gas sensors is to employ emerging two-dimensional (2D) materials with attractive properties such as high carrier mobility and large surface-to-volume ratios, which make them ideal materials for many applications in addition to gas sensing [14–27]. Several recent works have revealed that sensing devices based on graphene [12,28,29] or transition metal dichalcogenides (TMDs) like MoS<sub>2</sub> [30,31] can efficiently sense various gas molecules.

A number of recent theoretical and experimental studies have demonstrated the application of black phosphorene – the most stable allotrope of phosphorus – for gas sensing [32–41]. More recently, a new 2D phase of phosphorus with in-plane hexagonal structure called blue phosphorene (BlueP) has been designed theoretically [42] and synthesized experimentally [43]. BlueP has been found to be as stable as black phosphorene [31], and its narrow band gap makes it suitable for gas-sensing applications.

In this work, we employ density functional theory (DFT) calculations to predict the structural, electronic and VOCs sensing properties of BlueP monolayer upon defect engineering. Various types of point defects, i.e. mono-vacancy (MV-), di-vacancy (DV-), tri-vacancy (TV-), Si- and S-substitution, are considered, because they are known to affect the binding of molecules of 2D materials by making them electron-deficient

\* Corresponding author.

E-mail address: [tanveer.hussain@uwa.edu.au](mailto:tanveer.hussain@uwa.edu.au) (T. Hussain).<https://doi.org/10.1016/j.apsusc.2019.04.223>

Received 7 March 2019; Received in revised form 11 April 2019; Accepted 24 April 2019

Available online 02 May 2019

0169-4332/ © 2019 Elsevier B.V. All rights reserved.

or electron-rich. Indeed, all these defective BlueP monolayers show an improvement in the binding of VOCs (acetone, ethanol and propanal in this work) with respect to the pristine one, and major changes in electronic structure are observed for MV- and S-substituted BlueP monolayers, making them potential candidates for VOCs sensing.

## 2. Computational details

DFT calculations were performed using the VASP code [44] with the projector-augmented wave (PAW) pseudopotentials [45] and Perdew-Burke-Ernzerhof (PBE) gradient-corrected functionals [46]. Van der Waals interactions were treated by using the Grimme's method [47]. A cutoff energy of 600 eV for plane waves was used. Freestanding BlueP monolayer was modeled by a  $5 \times 5 \times 1$  hexagonal supercell consisting of 50 phosphorus atoms with a vacuum spacing of 25 Å along the z-direction to decouple the interaction between periodic replicas. The optimized lattice constant  $a_{hex}$  of BlueP monolayer is  $\sim 3.277$  Å. A  $4 \times 4 \times 1$  k-point mesh was used to sample the Brillouin zone. The electronic structure calculations are crosschecked by using the Heyd-Scuseria-Ernzerhof (HSE06) hybrid functionals [48], which in general enlarge the size of band gaps but do not lead to any qualitative difference with respect to GGA calculations. The data presented in the main text are all produced by GGA functionals, and some HSE calculations are shown in Figs. S1–S2.

## 3. Results and discussion

First of all, we perform DFT calculations to access the structural and electronic properties of pristine BlueP monolayer. The optimized structure of BlueP supercell is shown in Fig. 1(a), where P atoms are arranged in a planar hexagonal crystal lattice with two P atoms on one lattice point, similar to C atoms in graphene. The difference of BlueP from graphene is that the adjacent P atoms are not arranged in the same 2D plane, but instead they form an angle of  $92.92^\circ$ , not  $120^\circ$ . In other words, the monolayer is buckled, see the side view in Fig. 1(a). The bond length is calculated to be  $\sim 2.26$  Å, which agrees well with the experimental data [38].

To utilize BlueP as promising gas sensor for VOCs, two factors are important, a) a favorable binding of VOCs, and b) a major change in electronic structure before and after adsorption. The adsorption energies ( $E_{ads}$ ) for gas molecules (acetone, ethanol, and propanal in this work) are calculated by

$$E_{ads} = E_{BlueP+gas} - (E_{BlueP} + E_{gas}) \quad (1)$$

where, the first, second and third terms on the right-hand side refer to the total energy of the BlueP monolayer adsorbed with the gas molecules, bare BlueP, and the isolated VOC molecule, respectively. For each gas molecule, several configurations with different molecular orientations and adsorption sites (Fig. S3) are considered, and the configuration with the lowest energy is taken for further analysis (Fig. 2). The adsorption energies of BlueP monolayer for acetone, ethanol, and propanal are calculated to be favorable,  $-0.25$ ,  $-0.20$  and  $-0.26$  eV, respectively. However, the electronic structure of BlueP monolayers barely changes before and after the adsorption of these molecules, see the electronic density of states (DOS) in Fig. 2(d–f). This behavior makes gas sensing using pristine BlueP monolayers difficult.

Defect engineering using point defects, such as atomic vacancy and elemental substitution, is known as an effective route to alter the adsorption properties of 2D materials [27]. Here, we consider MV-, DV-, TV-, Si-, and S-BlueP monolayers (Fig. 1(b–f)) for adsorption of the acetone, ethanol, and propanal molecule. The adsorption energies are presented in Fig. 3(a). Clearly, all the considered point defects improve the binding of the acetone, ethanol, and propanal molecule, while the defect formation energies of DV- and TV-BlueP (Fig. 3(b)) are too high so that these two defective BlueP monolayers are more difficult for synthesis. Formation energies ( $E_f$ ) in case of vacancy defects and elemental substitutions in BlueP has been calculated by the following Eqs. (2) and (3), respectively

$$E_f = (E_{defected} + nE_P) - E_{pristine} \quad (2)$$

$$E_f = E_{A-BlueP} - [E_A + E_{(A-BlueP)-A}] \quad (3)$$

here  $E_f$  represents the formation energy;  $E_{defected}$  denotes the total energies of MV-BP, DV-BP, and TV-BP, for which  $n = 1, 2$ , and  $3$ , respectively;  $E_P$  represents the energy of an isolated P atom; and  $E_{pristine}$  is

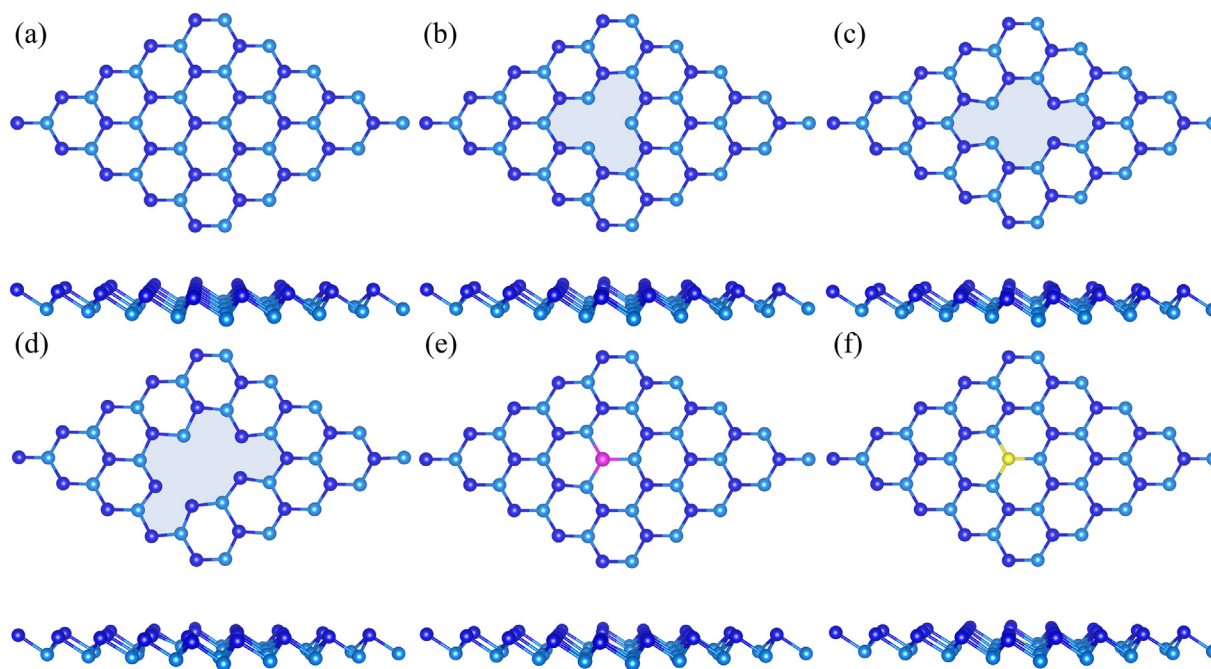


**Fig. 1.** Optimized structures (top and side views) of blue phosphorene monolayers: (a) Pristine (BlueP), (b) monovacancy (MV-BlueP), (c) divacancy (DV-BlueP), (d) trivacancy (TV-BlueP), (e) Si doped (Si-BlueP), and (f) S doped (S-BlueP). Atomic color scheme: P atoms in upper layer of BlueP, dark blue; P atoms in lower layer of BlueP, light blue; Si, purple; and S, yellow.

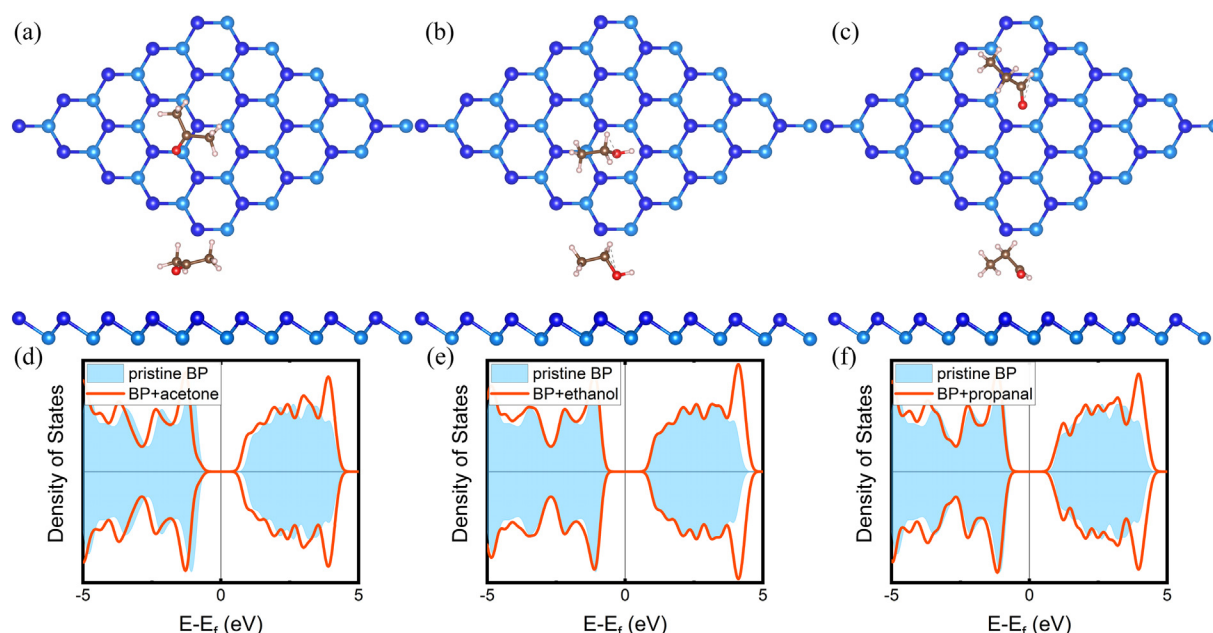


**Fig. 2.** Top and side views of the energetically most stable configurations of acetone (a), ethanol (b), and propanal (c) on BlueP, and their respective density of states (DOS) plots (e–f). Atomic color scheme: P atoms in upper layer of BlueP, dark blue; P atoms in lower layer of BlueP, light blue; H, pink; C, brown; and O, red.

the total energy of a pristine BlueP monolayer. Where  $A = \text{Si or S}$ ;  $E_A$  denotes the energy of an isolated  $A$  atom;  $E_{(A-\text{BlueP})-A}$  represents the energy of the residue of  $A$ -BP with  $A$  atom removed.

In the following, we investigate MV-, Si- and S-BlueP monolayer in more detail. First, we investigate the change in electronic structure upon creation of point defects without any molecule absorption. We calculate the charge density difference (CDD), spin-polarized DOS and band structure of the BlueP monolayers with and without point defects. The CDD plots presented in Fig. 4(a–c) clearly confirm a major change in charge distribution near the defect sites in the defective BlueP monolayers. In addition, MV and Si defects also create a couple of defect states within the band gap, while S defect moves the Fermi level to the tail of the conduction band (Fig. 4(d–f) and Fig. S4). These changes in electronic structure of defective BlueP monolayers should give rise to the change in their absorption properties.

Next, we study the changes in geometry and electronic structure of defective BlueP monolayers upon absorption of molecules. The

equilibrium distance of the three molecules with respect to the pristine, MV-, Si- and S-BlueP monolayer is summarized in Table 1. The much reduced equilibrium distance in the defective BlueP monolayers indicates the stronger binding of these molecules. The top and side views of the acetone, ethanol, and propanal molecule absorbed on the MV-, Si- and S-BlueP monolayer are presented in Fig. 5(a–c), Fig. 6(a–c) and Fig. 7(a–c). These geometrical configurations are used for the electronic structure calculations.

Regarding the MV-BlueP monolayer, a major change in electronic structure near the Fermi level is observed upon the absorption of the three molecules, as evidenced by the DOS (Fig. 5(d–f)) and band structure plots (Fig. S5). Before absorption, a couple of defect bands are found crossing the Fermi level, while upon absorption of the three molecules, such crossed bands split and shift away from the Fermi level (Fig. 5(d–f) and Fig. S5). Such change leads to a change in carrier concentration, which may result in a visible change in electrical conductivity that can be detected for sensing of these three molecules.

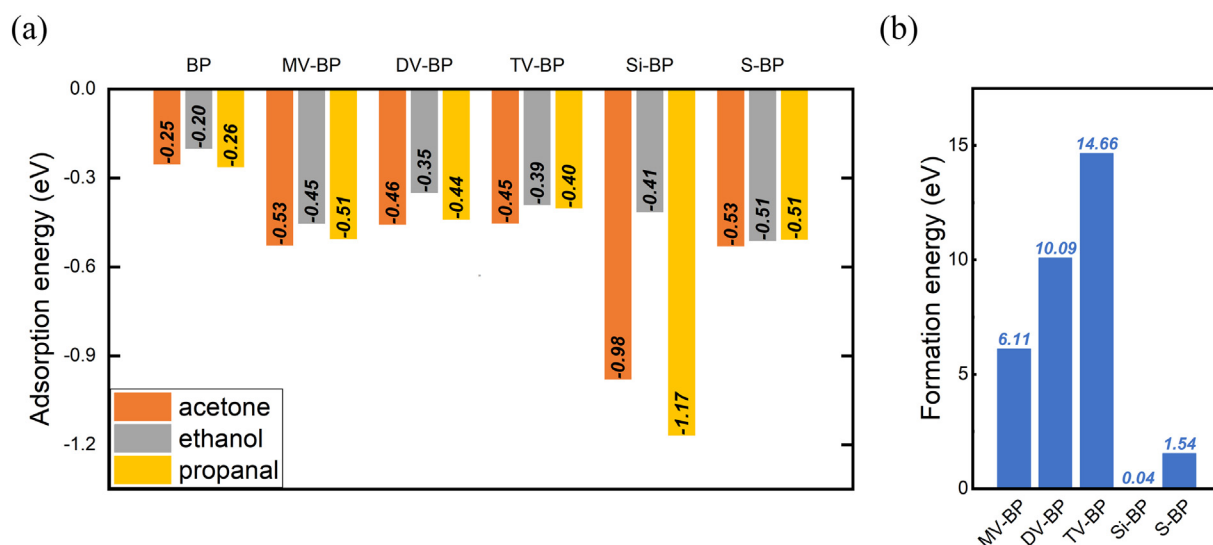


**Fig. 3.** (a) Adsorption energies of acetone, ethanol, and propanal on different BlueP monolayers; (b) Formation energies of defective BlueP sheets.

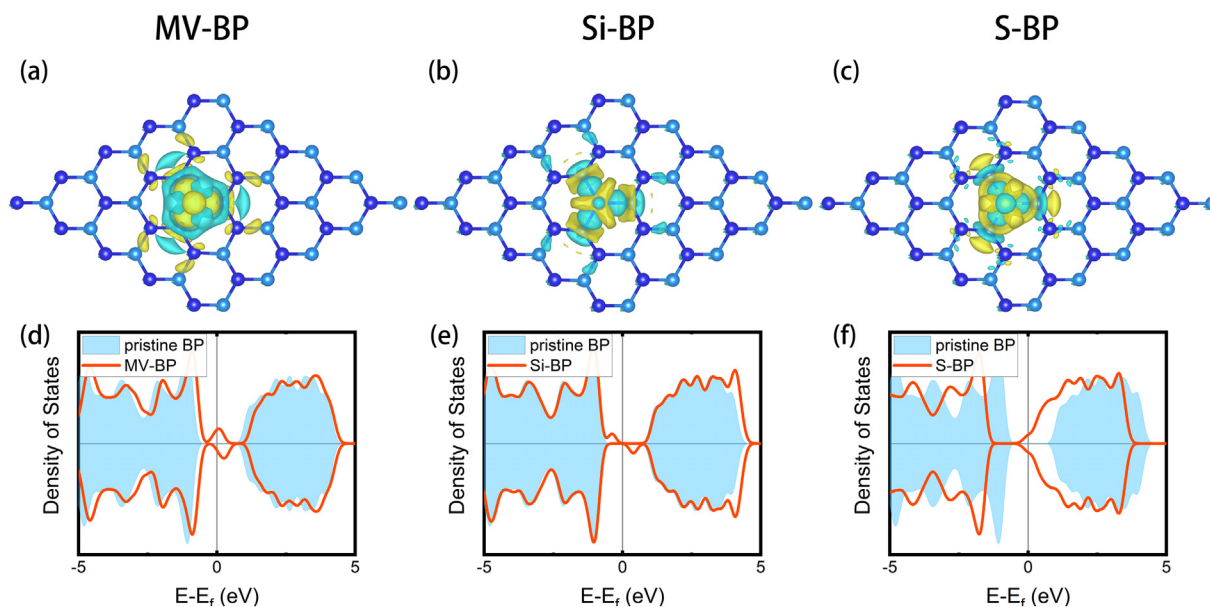


**Fig. 4.** Isosurface charge density of (a) MV-BP, (b) Si-BP, and (c) S-BP. Yellow and cyan surfaces represent the accumulation and depletion of charge, respectively, with isovalue of  $0.01 \text{ e}/\text{\AA}^3$ . (d)–(f): DOS of MV-BP, Si-BP, and S-BP (red line) along with pristine BlueP (cyan filling).

**Table 1**

Equilibrium bond distances (in  $\text{\AA}$ ) between VOC molecules and BlueP monolayers after relaxations along z-axis.

	BP	MV-BP	Si-BP	S-BP
Acetone	3.02	1.57	1.26	2.73
Ethanol	2.69	1.85	2.02	2.54
Propanal	2.94	1.56	1.14	2.88

As regards the other electron-deficient BlueP monolayer, Si-BlueP shows one pair of spin-up and spin-down defect bands near the Fermi level, while they do not cross the Fermi level (Fig. S6(a)). Marginal change in DOS and band structure is found upon the absorption of ethanol, while the spin-down band is no longer found near the Fermi

level upon the absorption of acetone and propanal (Fig. 6(d–f) and Fig. S6). The vanishing of the spin-down middle gap band may also lead to some change in carrier concentration and thereby electrical conductivity, but such change should be much smaller than that of the MV-BlueP case.

For S-BlueP monolayer, the S substitution provides one more *p* electron, which shifts the Fermi level towards the conduction band. The pair of spin-up and spin-down bands brought by this additional electron appears near the conduction band and crosses the Fermi level (Fig. S7(a)). Upon absorption of the three molecules, the Fermi level is shifted towards the middle of the band gap, and the defect bands no longer cross the Fermi level. Such major change in electronic structure should render S-BlueP monolayer as a suitable candidate for the sensing of these three molecules.

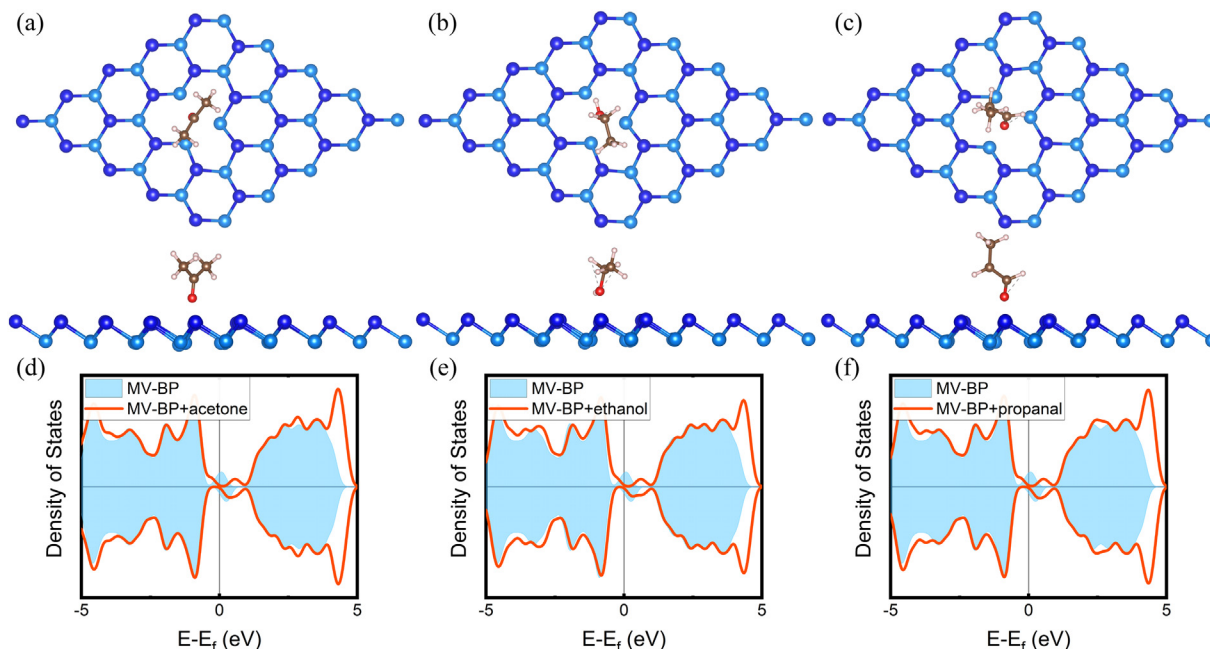


**Fig. 5.** Top and side view of the most stable configurations of acetone (a), ethanol (b), and propanal (c) on MV-BP, and their respective density of states (DOS) plots (d–f). Atomic color scheme: P atoms in upper layer of BlueP, dark blue; P atoms in lower layer of BlueP, light blue; H, pink; C, brown; and O, red.

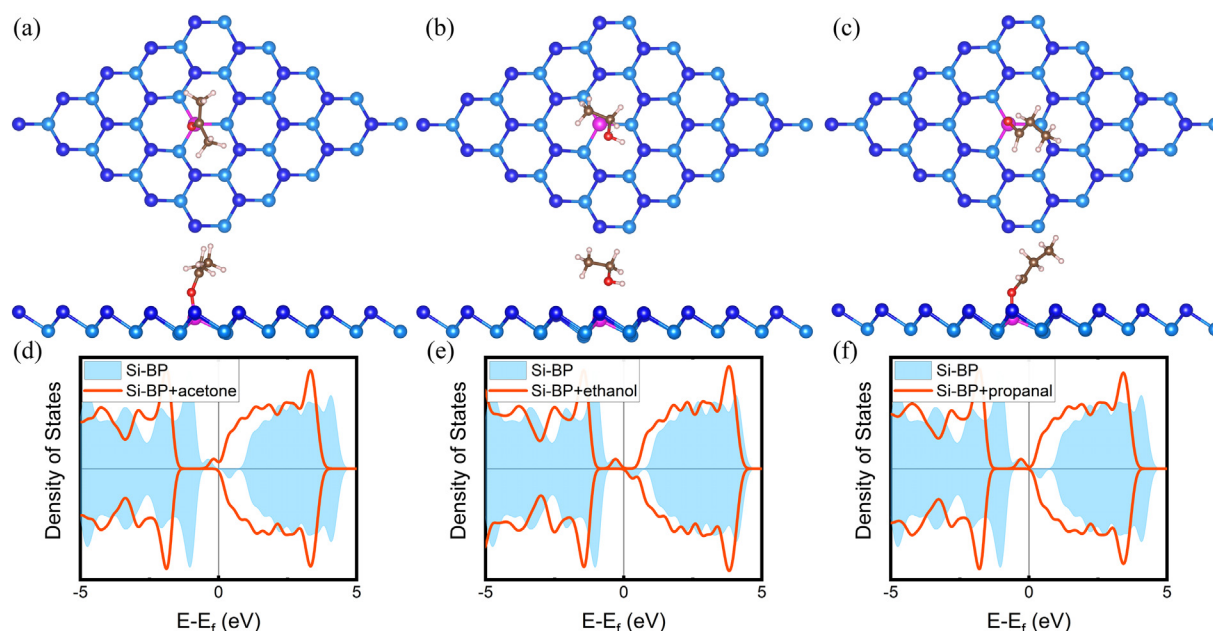


Fig. 6. Top and side views of the most stable configurations of acetone (a), ethanol (b), and propanal (c) on Si-BlueP, and their respective density of states (DOS) plots (d–f). Atomic color scheme: P atoms in upper layer of BlueP, dark blue; P atoms in lower layer of BlueP, light blue; H, pink; C, brown; and O, red; and Si, purple.

#### 4. Conclusions

Spin-polarized DFT calculations were carried out to investigate the structural, electronic, and sensing characteristics of pristine, MV- and Si/S-doped blue phosphorene monolayer with and without the absorption of volatile organic molecules, including acetone, ethanol, and propanal. Our energy analysis reveals favorable absorption tendency of the three molecules by pristine BlueP, however, the marginal change in electronic structure rules out pristine BlueP as potential gas nanosensors. The binding energy of between the three molecules and BlueP monolayer significantly increases upon the formation of vacancies and element substitution. The relatively low formation energy of mono-

vacancy, Si and S substitution (within a  $5 \times 5$  supercell of BlueP monolayer) makes these defective BlueP monolayers potentially feasible for synthesis. Moreover, major changes in electronic structure before and after the absorption of the three molecules are found in the MV- and S-BlueP monolayer, which shall lead to detectable changes in electrical conductivity, suggesting these two defective BlueP monolayers to be potentially good gas nanosensors.

Supplementary data to this article can be found online at <https://doi.org/10.1016/j.apsusc.2019.04.223>.

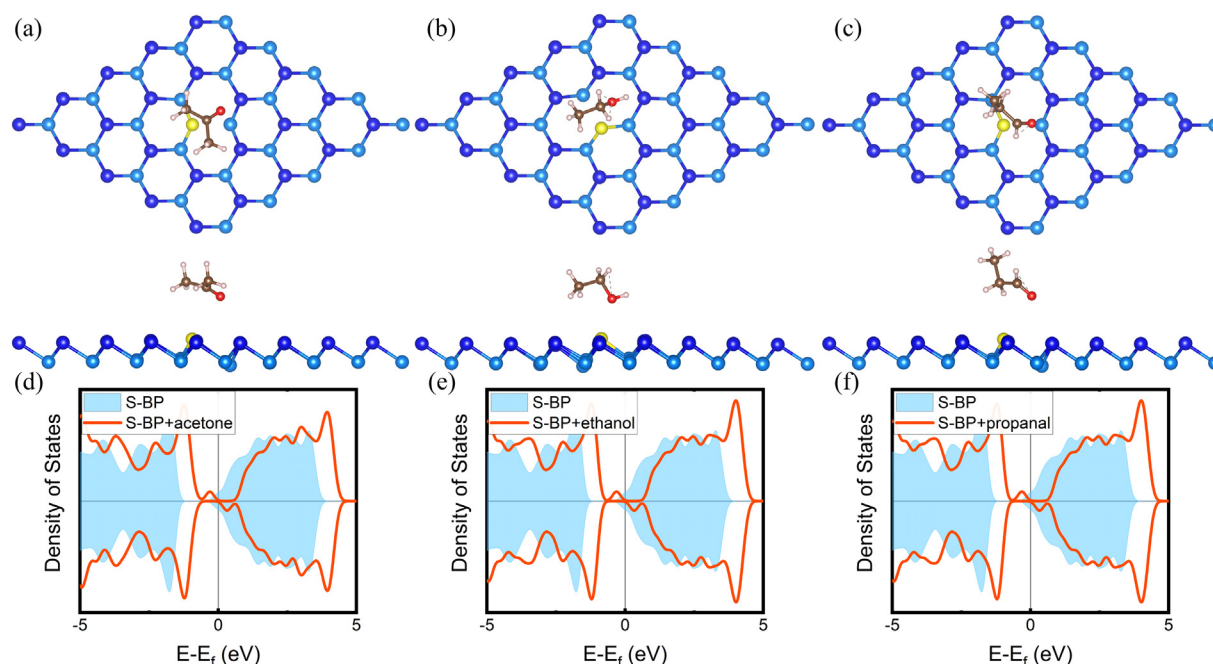


Fig. 7. Top and side views of the most stable configurations of acetone (a), ethanol (b), and propanal (c) on S-BlueP, and their respective density of states (DOS) plots (d–f). Atomic color scheme: P atoms in upper layer of BlueP, dark blue; P atoms in lower layer of BlueP, light blue; H, pink; C, brown; and O, red; and S, yellow. (For interpretation of the references to color in this figure legend, the reader is referred to the web version of this article.)

## Acknowledgements

This research was undertaken with the assistance of computational resources at the HPC platform of Xi'an Jiaotong University and the Linux cluster of the Karton group at the University of Western Australia. We gratefully acknowledge the provision of an Australian Research Council (ARC) Future Fellowship (to A.K.; Project No. FT170100373). The support of the International Joint Laboratory for Micro/Nano Manufacturing and Measurement Technologies (IJL-MMMT) of Xi'an Jiaotong University is also acknowledged.

## References

- [1] H. Guo, S.C. Lee, L.Y. Chan, W.M. Li, Risk assessment of exposure to volatile organic compounds in different indoor environments, *Environ. Res.* 94 (2004) 57–66, [https://doi.org/10.1016/s0013-9351\(03\)00035-5](https://doi.org/10.1016/s0013-9351(03)00035-5).
- [2] T. Salthammer, Very volatile organic compounds: an understudied class of indoor air pollutants, *Indoor Air* 26 (2016) 25–38, <https://doi.org/10.1111/ina.12173>.
- [3] S. Wang, H.M. Ang, M.O. Tade, Volatile organic compounds in indoor environment and photocatalytic oxidation: state of the art, *Environ. Int.* 33 (2007) 694–705, <https://doi.org/10.1016/j.envint.2007.02.011>.
- [4] L. Molhave, Volatile organic compounds, indoor air quality and health, *Indoor Air* 1 (1991) 357–376, <https://doi.org/10.1111/j.1600-0668.1991.00001.x>.
- [5] J. Bartzis, P. Wolkoff, M. Stranger, G. Efthimiou, E.I. Tolis, F. Maes, A.W. Norgaard, G. Ventura, K.K. Kalimeri, E. Goelen, O. Fernandes, On organic emissions testing from indoor consumer products' use, *J. Hazard. Mater.* 285 (2015) 37–45, <https://doi.org/10.1016/j.jhazmat.2014.11.024>.
- [6] A. Mirzaei, S.G. Leonardi, G. Neri, Detection of hazardous volatile organic compounds (VOCs) by metal oxide nanostructures-based gas sensors: a review, *Ceram. Int.* 42 (2016) 15119–15141, <https://doi.org/10.1016/j.ceramint.2016.06.145>.
- [7] A.P. Dral, J.E. ten Elshof, 2D metal oxide nanoflakes for sensing applications: review and perspective, *Sensors Actuators B Chem.* 272 (2018) 369–392, <https://doi.org/10.1016/j.snb.2018.05.157>.
- [8] S. Gupta Chatterjee, S. Chatterjee, A.K. Ray, A.K. Chakraborty, Graphene–metal oxide nanohybrids for toxic gas sensor: a review, *Sensors Actuators B Chem.* 221 (2015) 1170–1181, <https://doi.org/10.1016/j.snb.2015.07.070>.
- [9] Z. Zhang, X. Zou, L. Xu, L. Liao, W. Liu, J. Ho, X. Xiao, C. Jiang, J. Li, Hydrogen gas sensor based on metal oxide nanoparticles decorated graphene transistor, *Nanoscale* 7 (2015) 10078–10084, <https://doi.org/10.1039/c5nr01924a>.
- [10] G.B.S.V.E. Bochenkov, Sensitivity, Selectivity, and Stability of Gas-Sensitive Metal-Oxide Nanostructures, *Metal Oxide Nanostructures and Their Applications*, (2010), p. 3.
- [11] S. Capone, A. Forleo, L. Francioso, R. Rella, P. Siciliano, J. Spadavecchia, D.S. Presicce, A.M. Taurino, Solid state gas sensors: state of the art and future activities, *J. Optoelectron. Adv. Mater.* 5 (2003) 1335–1348.
- [12] F. Schedin, A.K. Geim, S.V. Morozov, E.W. Hill, P. Blake, M.I. Katsnelson, K.S. Novoselov, Detection of individual gas molecules adsorbed on graphene, *Nat. Mater.* 6 (2007) 652–655, <https://doi.org/10.1038/nmat1967>.
- [13] M. Karmaoui, S.G. Leonardi, M. Latino, D.M. Tobaldi, N. Donato, R.C. Pullar, M.P. Seabra, J.A. Labrincha, G. Neri, Pt-decorated In<sub>2</sub>O<sub>3</sub> nanoparticles and their ability as a highly sensitive (< 10 ppb) acetone sensor for biomedical applications, *Sensors Actuators B Chem.* 230 (2016) 697–705, <https://doi.org/10.1016/j.snb.2016.02.100>.
- [14] A.H. Farokh Niaei, T. Hussain, M. Hankel, D.J. Searles, Hydrogenated defective graphene as an anode material for sodium and calcium ion batteries: a density functional theory study, *Carbon* 136 (2018) 73–84, <https://doi.org/10.1016/j.carbon.2018.04.034>.
- [15] T. Hussain, A. De Sarkar, R. Ahuja, Functionalization of hydrogenated graphene by polythiated species for efficient hydrogen storage, *Int. J. Hydrog. Energy* 39 (2014) 2560–2566, <https://doi.org/10.1016/j.ijhydene.2013.11.083>.
- [16] X. Zhou, Q. Zhang, L. Gan, H. Li, J. Xiong, T. Zhai, Booming development of group IV–VI semiconductors: fresh blood of 2D family, *Adv. Sci. (Weinh)* 3 (2016) 1600177, <https://doi.org/10.1002/adv.201600177>.
- [17] S. Manzeli, D. Ovchinnikov, D. Pasquier, O.V. Yazyev, A. Kis, 2D transition metal dichalcogenides, *Nat. Rev. Mater.* 2 (2017), <https://doi.org/10.1038/natrevmats.2017.33>.
- [18] J.R. Schaibley, H. Yu, G. Clark, P. Rivera, J.S. Ross, K.L. Seyler, W. Yao, X. Xu, Valleytronics in 2D materials, *Nat. Rev. Mater.* 1 (2016), <https://doi.org/10.1038/natrevmats.2016.55>.
- [19] Q.H. Wang, K. Kalantar-Zadeh, A. Kis, J.N. Coleman, M.S. Strano, Electronics and optoelectronics of two-dimensional transition metal dichalcogenides, *Nat. Nanotechnol.* 7 (2012) 699–712, <https://doi.org/10.1038/nnano.2012.193>.
- [20] J. Wang, I. Ronneberger, L. Zhou, L. Lu, V.L. Deringer, B. Zhang, L. Tian, H. Du, C. Jia, X. Qian, M. Wuttig, R. Mazzarello, W. Zhang, Unconventional two-dimensional germanium dichalcogenides, *Nanoscale* 10 (2018) 7363–7368, <https://doi.org/10.1039/c8nr01747f>.
- [21] J. Zhou, Q. Sun, G. Wang, P. Jena, High-temperature superconductivity in heavily N- or B-doped graphene, *Phys. Rev. B* 92 (2015), <https://doi.org/10.1103/PhysRevB.92.064505>.
- [22] Chandiramouli Nagarajan, Nitrogen dioxide and ammonia gas molecules interaction studies on phosphorene nanosheet — a DFT investigation, *Condens. Matter Phys.* 22 (2019), <https://doi.org/10.5488/cmp.22.13703>.
- [23] V. Nagarajan, R. Chandiramouli, Probing cyanogen chloride gas molecules using blue phosphorene nanosheets based on adsorption properties: a first-principles study, *Comput. Theor. Chem.* 1150 (2019) 63–70, <https://doi.org/10.1016/j.comptc.2019.01.013>.
- [24] P. Snehha, V. Nagarajan, R. Chandiramouli, Interaction behavior of cyanogen fluoride and chloride gas molecules on red phosphorene nanosheet: a DFT study, *J. Inorg. Organomet. Polym. Mater.* (2019), <https://doi.org/10.1007/s10904-018-01070-3>.
- [25] R. Bhuvaneshwari, R. Chandiramouli, First-principles investigation on detection of phosgene gas molecules using phosphorene nanosheet device, *Chem. Phys. Lett.* 717 (2019) 99–106, <https://doi.org/10.1016/j.cplett.2019.01.018>.
- [26] D. John, R. Chatanathodi, Hydrogen adsorption on alkali metal decorated blue phosphorene nanosheets, *Appl. Surf. Sci.* 465 (2019) 440–449, <https://doi.org/10.1016/j.apsusc.2018.09.158>.
- [27] F. Safari, M. Moradinasab, M. Fathipour, H. Kosina, Adsorption of the NH<sub>3</sub>, NO, NO<sub>2</sub>, CO<sub>2</sub>, and CO gas molecules on blue phosphorene: a first-principles study, *Appl. Surf. Sci.* 464 (2019) 153–161, <https://doi.org/10.1016/j.apsusc.2018.09.048>.
- [28] B. Huang, Z. Li, Z. Liu, G. Zhou, S. Hao, J. Wu, B.-L. Gu, W. Duan, Adsorption of gas molecules on graphene nanoribbons and its implication for nanoscale molecule sensor, *J. Phys. Chem. C* 112 (2008) 13442–13446, <https://doi.org/10.1021/jp8021024>.
- [29] Y.H. Zhang, Y.B. Chen, K.G. Zhou, C.H. Liu, J. Zeng, H.L. Zhang, Y. Peng, Improving gas sensing properties of graphene by introducing dopants and defects: a first-principles study, *Nanotechnology* 20 (2009) 185504, <https://doi.org/10.1088/0957-4484/20/18/185504>.
- [30] X.-Q. Tian, L. Liu, X.-R. Wang, Y.-D. Wei, J. Gu, Y. Du, B.I. Yakobson, Engineering of the interactions of volatile organic compounds with MoS<sub>2</sub>, *J. Mater. Chem. C* 5 (2017) 1463–1470, <https://doi.org/10.1039/c6tc04673h>.
- [31] D. Sarkar, X. Xie, J. Kang, H. Zhang, W. Liu, J. Navarrete, M. Moskovits, K. Banerjee, Functionalization of transition metal dichalcogenides with metallic nanoparticles: implications for doping and gas-sensing, *Nano Lett.* 15 (2015) 2852–2862, <https://doi.org/10.1021/nl504454u>.
- [32] L. Li, Y. Yu, G.J. Ye, Q. Ge, X. Ou, H. Wu, D. Feng, X.H. Chen, Y. Zhang, Black phosphorus field-effect transistors, *Nat. Nanotechnol.* 9 (2014) 372–377, <https://doi.org/10.1038/nnano.2014.35>.
- [33] L. Kou, T. Frauenheim, C. Chen, Phosphorene as a superior gas sensor: selective adsorption and distinct I-V response, *J. Phys. Chem. Lett.* 5 (2014) 2675–2681, <https://doi.org/10.1021/jz501188k>.
- [34] A.N. Abbas, B. Liu, L. Chen, Y. Ma, S. Cong, N. Aronyadet, M. Kopf, T. Nilges, C. Zhou, Black phosphorus gas sensors, *ACS Nano* 9 (2015) 5618–5624, <https://doi.org/10.1021/acsnano.5b01961>.
- [35] Q. Yang, R.-S. Meng, J.-K. Jiang, Q.-H. Liang, C.-J. Tan, M. Cai, X. Sun, D.-G. Yang, T.-L. Ren, X.-P. Chen, First-principles study of sulfur dioxide sensor based on phosphorene, *IEEE Electron Device Lett.* 37 (2016) 660–662, <https://doi.org/10.1109/led.2016.2543243>.
- [36] T. Kaewmaraya, L. Ngamwongwan, P. Moontragoon, A. Karton, T. Hussain, Drastic improvement in gas-sensing characteristics of phosphorene nanosheets under vacancy defects and elemental functionalization, *J. Phys. Chem. C* (2018), <https://doi.org/10.1021/acs.jpcc.8b06803>.
- [37] A.-J. Yang, D.-W. Wang, X.-H. Wang, J.-F. Chu, P.-L. Lv, Y. Liu, M.-Z. Rong, Phosphorene: a promising candidate for highly sensitive and selective SF<sub>6</sub> decomposition gas sensors, *IEEE Electron Device Lett.* 38 (2017) 963–966, <https://doi.org/10.1109/led.2017.2701642>.
- [38] H. Liu, A.T. Neal, Z. Zhu, Z. Luo, X. Xu, D. Tomanek, P.D. Ye, Phosphorene: an unexplored 2D semiconductor with a high hole mobility, *ACS Nano* 8 (2014) 4033–4041, <https://doi.org/10.1021/nn501226z>.
- [39] M.S. Mahabal, M.D. Deshpande, T. Hussain, R. Ahuja, Sensing characteristics of phosphorene monolayers toward PH<sub>3</sub> and AsH<sub>3</sub> gases upon the introduction of vacancy defects, *J. Phys. Chem. C* 120 (2016) 20428–20436, <https://doi.org/10.1021/acs.jpcc.6b06791>.
- [40] S. Balendhran, S. Walia, H. Nili, S. Sriram, M. Bhaskaran, Elemental analogues of graphene: silicene, germanene, stanene, and phosphorene, *Small* 11 (2015) 640–652, <https://doi.org/10.1002/smll.201402041>.
- [41] L. Kou, C. Chen, S.C. Smith, Phosphorene: fabrication, properties, and applications, *J. Phys. Chem. Lett.* 6 (2015) 2794–2805, <https://doi.org/10.1021/acs.jpclett.5b01094>.
- [42] Z. Zhu, D. Tomanek, Semiconducting layered blue phosphorus: a computational study, *Phys. Rev. Lett.* 112 (2014) 176802, <https://doi.org/10.1103/PhysRevLett.112.176802>.
- [43] J.L. Zhang, S. Zhao, C. Han, Z. Wang, S. Zhong, S. Sun, R. Guo, X. Zhou, C.D. Gu, K.D. Yuan, Z. Li, W. Chen, Epitaxial growth of single layer blue phosphorus: a new phase of two-dimensional phosphorus, *Nano Lett.* 16 (2016) 4903–4908, <https://doi.org/10.1021/acs.nanolett.6b01459>.
- [44] G. Kresse, J. Furthmüller, Efficient iterative schemes for ab initio total-energy calculations using a plane-wave basis set, *Phys. Rev. B* 54 (1996) 11169–11186, <https://doi.org/10.1103/PhysRevB.54.11169>.
- [45] P.E. Blochl, Projector augmented-wave method, *Phys. Rev. B Condens. Matter* 50 (1994) 17953–17979, <https://doi.org/10.1103/PhysRevB.50.17953>.
- [46] J.P. Perdew, K. Burke, M. Ernzerhof, Generalized gradient approximation made simple, *Phys. Rev. Lett.* 77 (1996) 3865–3868, <https://doi.org/10.1103/PhysRevLett.77.3865>.
- [47] S. Grimme, Semiempirical GGA-type density functional constructed with a long-range dispersion correction, *J. Comput. Chem.* 27 (2006) 1787–1799, <https://doi.org/10.1002/jcc.20495>.
- [48] J. Paier, M. Marsman, K. Hummer, G. Kresse, I.C. Gerber, J.G. Angyan, Screened hybrid density functionals applied to solids, *J. Chem. Phys.* 124 (2006) 154709, <https://doi.org/10.1063/1.2187006>.